Toward Real-time Penetrating Imaging Radar at 670 GHz

R. J. Dengler[1], K. B. Cooper[1], N. Llombart[1], G. Chattopadhyay[1], T. Bryllert[1], I. Mehdi[1], P. H. Siegel[1,2]

[1]Jet Propulsion Laboratory, California Institute of Technology, Pasadena, CA 91109, USA
[2]Dept. of Biology, California Institute of Technology, Pasadena, CA 91125, USA

***Abstract* — Since the first report on our submillimeter-wave imaging system with radar ranging capabilities, several advances have been made in system performance. Range resolution as well as cross-range resolution are significantly improved, and image acquisition time has been reduced from over 5 minutes to under 1 minute. Here we report on performance improvements to specific key components and software that yielded these results. Further advances in these and other components will be discussed that we expect will enable, for the first time ever, near real-time 3D radar imaging at THz wavelengths.**

***Index Terms* — Submillimeter wave imaging, FMCW chirp radar, submillimeter wave radar, radar imaging, submillimeter chirp, THz radar.**

I. Introduction

The system discussed in this paper is an active single-pixel scanned imager operating at 670 GHz and is based on the system described in detail in [1]. The actual chirp signals for the RF and LO chains were generated by a pair of Miteq 2.5-3.3 GHz chirp sources. Agilent benchtop synthesizers operating at fixed frequencies around 13 GHz were then used to upconvert the chirp sources to 15.5-16.3 GHz. The resulting signals were then multiplied 36 times by a combination of off-the shelf millimeter wave components and JPL-built 200 GHz doublers and 300 GHz and 600 GHz triplers [2]. The power required to drive the submillimeter wave multipliers was provided by JPL-built W-band amplifiers [3, 4]. The receive and transmit signal paths were combined using a thin high resistivity silicon wafer as a beam splitter.

While the results presented in [1] are encouraging, the system still lacks sufficient image acquisition speed to be usable for practical applications in contraband detection. Ideally, an image acquisition speed of 10 seconds, or a factor of 30 improvement from [1], is desired. In this paper we focus on the system improvements that have resulted to date in a factor of 5 increase in image acquisition speed, as well as enhanced signal processing algorithms, permitting clearer imaging of contraband objects hidden underneath clothing. In particular, advances in three distinct areas have enabled these performance enhancements: base source phase noise reduction, chirp rate, and signal processing. Additionally, a second pixel was added, automatically reducing the imaging time by a factor of two.

II. Chirp Sources

The chirp speed used in [1] was limited in part by the signal to noise ratio of the system. Because of the high multiplication ratio used (×36), the primary factor limiting the dynamic range was not receiver noise figure or lack of transmitter power, but phase noise in the transmitted and LO signals. In order to reduce this noise, a lower multiplication factor of ×18 was chosen. In order to generate the base chirp signals, a pair of very low noise 35 GHz synthesizers from Miteq was employed. These synthesizers were then used to upconvert a new chirp source. Since the new multiplication factor was half of the previous value, the required bandwidth of the chirper was greater than that of the previous unit. For ×18 multiplication and 29 GHz chirp bandwidth, a base chirp bandwidth of ~1.6 GHz was required. Additionally, in order to keep the wide band phase noise contribution from the chirp source as low as possible, the lowest possible frequency range that still yielded a 1.6 GHz chirp band was chosen. A Mini-Circuits ROS-3200-419+ was chosen as the VCO for the chirper due to its low cost, wide full-octave bandwidth and low operating frequency. Its phase noise at frequency offsets above 1 MHz is 15 to 20 dB lower than higher frequency wideband VCOs.

While reduced phase noise is important to improving the signal to noise ratio, this reduced noise must be maintained while chirping at a fast rate. In order to ultimately achieve near real-time imaging speeds using a reasonably small

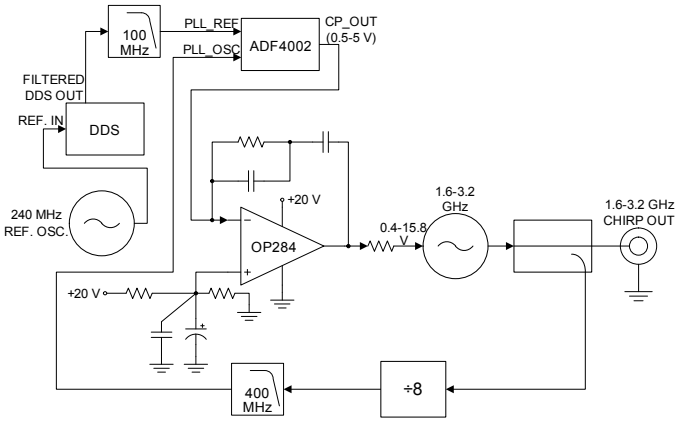

Figure 1. Block diagram of chirp source.

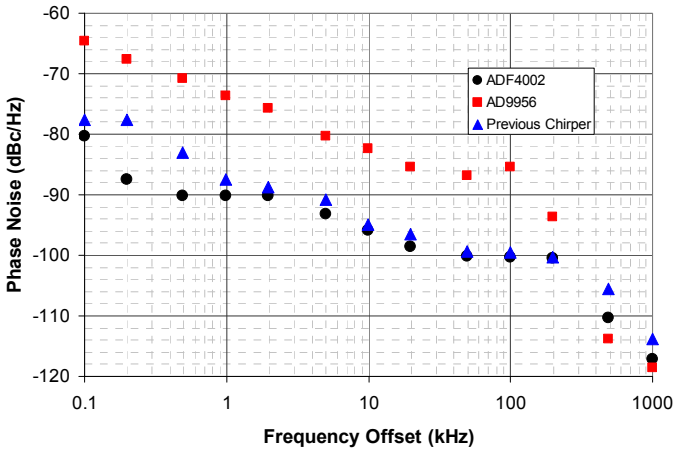

Figure 2. Comparison of phase noise of chirp sources using ADF4002 and AD9956 (integrated DDS/phase detector). The chirp sources were in single frequency mode. Note the 15 to 20 dB improvement in phase noise of the ADF4002-based source as compared to the AD9956-based chirper; this is due to the 26 dB difference in phase detector noise floor between the two units. Also shown for comparison is the phase noise of the Miteq chirper used in [1]. The reference source used for the ADF4002-based chirper in this measurement was an Agilent E4400B synthesizer, which was found to contribute a small amount of phase noise in the 1-5 kHz offset region.

number of parallel transceiver channels, a single chirped pulse must be acquired in 1 millisecond or less. This represents a factor of 12 decrease in chirp duration over the previous design, with a chirp rate of roughly double the increase in duration due to the halving of the base source multiplication factor. While the chirp source in the old system ran at a 0.064 MHz/µsec. chirp rate, the new chirper was required to operate at 1.6 MHz/µsec. These requirements were achieved using a hybrid PLL/DDS design shown in Fig. 1. In order to keep implementation costs down and minimize design cycle time, the 1.6-3.2 GHz chirper was designed using vendor-assembled evaluation boards for the VCO, DDS, microwave divider and phase detector/PLL. The DDS board reference was driven from the same ultra low-noise 240 MHz reference oscillator feeding the Miteq synthesizers in order to obtain the lowest possible phase noise output from the DDS, which was used as the reference input for the PLL section. The phase detector/PLL device chosen, an Analog Devices ADF4002 has the lowest normalized phase noise floor (-222 dBc/Hz) of

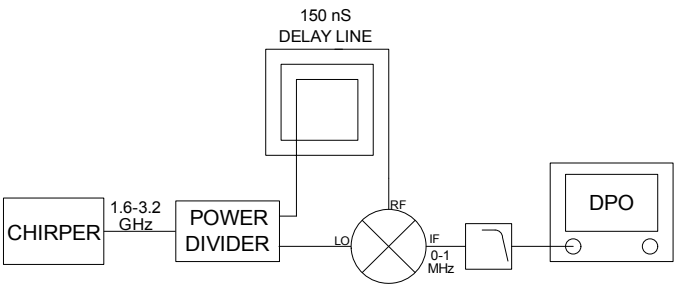

Figure 3. Block diagram of test system for chirp source.

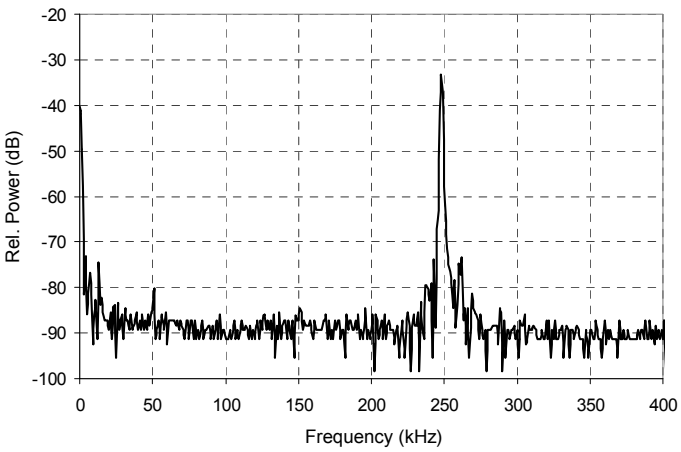

Figure 4. IF spectrum of chirp source operated at 1.6 MHz/µsec. using measurement system of Fig. 3. The –40 dBc peak ~15 kHz above the main peak is due to reflections between the power divider and actual source VCO within the chirper. The measured 3 dB bandwidth of 1 kHz (twice the resolution bandwidth of the FFT) confirms the high linearity of the chirp.

all their products at the time of this writing [5]. Since the VCO requires a tuning voltage of 0-20 V while the charge pump output from the ADF4002's phase detector only supplies 5 V, an active loop filter was designed using SimPLL [6]. In addition to providing the DC gain required to drive the VCO's tuning input across its entire range, the loop filter was optimized for low phase noise while maintaining sufficient loop bandwidth to maintain phase lock during chirping. Fig. 2 illustrates the phase noise performance of the chirp source compared with other implementations.

As previously mentioned, it is critical that a chirp source maintain good phase noise performance while actually chirping. To verify that the new design meets this criterion, a simulated radar testbed was assembled as illustrated in Fig. 3. A difference in path length of 150 ns between the LO and RF ports of the mixer was generated by a 31 meter length of semi-rigid coax. The resulting IF output frequency is a function of chirp speed given by

$$f_{IF} = KT \qquad (1)$$

where K is the chirp rate in MHz/µs and T is the path time difference between the LO and RF ports in seconds. A Tektronix digital phosphor oscilloscope with FFT firmware was used as the detector. Fig. 4 illustrates the purity of the chirp source as well as the high linearity, which is an inherent feature of the hybrid DDS design.

III. Signal Processing

The imaging THz radar system is controlled by a PC running software written in LabVIEW. Originally, much of the signal processing code was written using the LabVIEW-Mathscript language. However, processing overhead in the LabVIEW-Mathscript linkage prevented pixel acquisition

TABLE I
Labview Execution Time for IIR Low-pass Zero-phase Filtering/Decimation of 32000 Double Precision Datapoints (values in milliseconds)

Filter Implementation/ CPU speed and type	Mathscript Node	LabVIEW	C DLL
2.67 GHz Pentium 4 (“Northwood”)	52	13.3	9.8
3 GHz Pentium D (“Presler”)	43.5	6.5	4.5
2.8 GHz Core 2 Quad (“Yorkfield”)	12.0	2.81	2.31

times faster than ~50 ms/pixel. This problem was remedied by removing all MathScript code nodes from the signal processing code and replacing them using only native LabVIEW signal processing VIs. Other speed bottlenecks in the signal processing were eliminated by using more streamlined coding - for example by running a peak-detection algorithm on only the subset of the compressed range data occupied by the target. This left the computation-intensive low pass IIR filter/decimator as the primary “choke point” of our current radar signal processing algorithm, and we tested the further optimization of this process by utilizing code written in C, compiled as Windows executable dynamic link libraries (DLLs). These C modules could be optimized to achieve faster performance than could be attained by using the more generalized LabVIEW libraries. For example, benchmarking of the low pass IIR filter/decimator is presented in Table 1. Note that both LabVIEW and C implementations benefit from multiprocessing, as the execution speed scales inversely with the number of available processor cores (the “Presler” CPU has 2 cores, and the “Yorkfield” CPU has 4). In a future near video-rate imaging radar system, we expect these C modules to be imported onto a fast embedded processor, or that they be adapted to an FPGA-based signal processing platform.

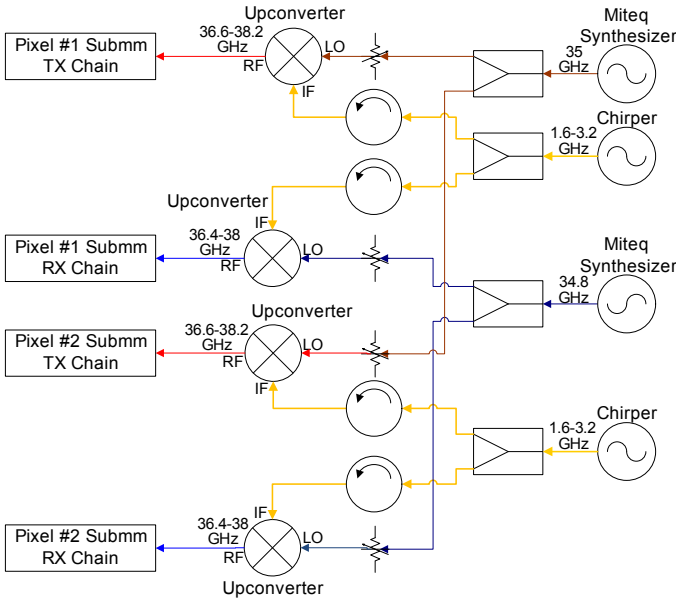

Figure 5. Block diagram of base signal source distribution for 2 pixel imaging system.

IV. Addition of Second Pixel

Additional transceiving elements decrease the image acquisition time without decreasing individual pixel acquisition time. Although adding a second pixel to the system doubles the amount of submillimeter components required, some savings in microwave hardware can be realized by using a common low noise source. In Fig. 5 the low noise transmit and LO synthesizer signals are divided and sent to both pixels, while each pixel maintains its own chirp source. By applying an asynchronous chirp signal generated by independent chirpers to each pixel, cross coupling between the pixels is completely eliminated. This has the added benefit of eliminating an undesired modulation problem within the base signal generating subsystem: the power dividers fed by each synthesizer have limited isolation, allowing mixing products from one upconverter to leak out of its LO input and back into the LO input of the other pixel’s upconverter. When the chirps for each pixel are temporally correlated, this leakage causes subtle phase and amplitude shifts in the base transmit signals at the output of the upconverters, leading to loss of range resolution caused by “smearing” of the demodulated spectrum. By decorrelating the two chirp signals, these products fall outside the final IF range of the receivers. Although additional isolators at the outputs of the power dividers would also remedy this problem, the use of independent asynchronous chirpers for each pixel affords the additional benefit of eliminating any cross coupling between the beam patterns of closely spaced pixels (the two pixels in our system are separated by about 18 3 dB beamwidths, corresponding to 10 cm at 4 m standoff distance, so this was not an issue here). Since proper detection requires that the LO chirp be phase matched to the transmit signal, each chirper is able to supply signal for both the transmit and LO upconverters for its associated pixel. Low cost 1.5-3.5 GHz isolators on the chirper power divider outputs prevent cross coupling between the IF ports of the transmit and LO upconverters.

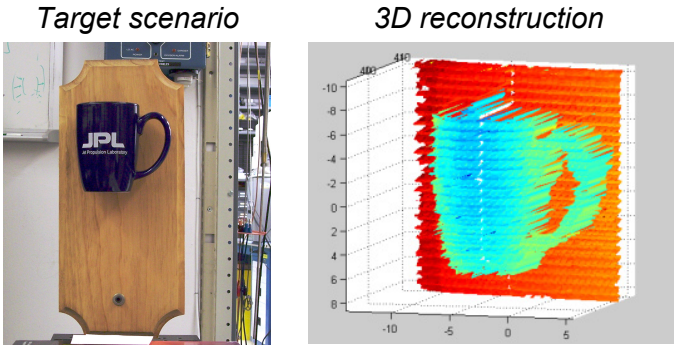

Figure 6. Picture of coffee mug and submillimeter 3D reconstruction of mug. Each half of the mug was imaged with one of the two pixels.

We are currently working on fully optimizing the imaging capabilities of the dual-transceiver system, and an early result is shown in Figure 6 where a coffee mug at 4 m standoff was imaged. With a transmitted chirp bandwidth of 14.4 GHz and a chirp time of 6 ms, the complete 9,936-pixel radar image required about 52 seconds to acquire. The primary speed bottleneck of this image was not the chirp time, which was not fully optimized for this test, but rather the large mechanical stage used to scan the radar beam across the mug.

V. Conclusion

Considerable progress has been made in transforming our original 600 GHz imaging radar system from a laboratory testbed apparatus into an instrument that can be deployed into the real world for use in security applications. Development of optical multiplexing techniques promises to synthesize additional pixels without increasing the number of transceivers, however further enhancements in signal processing speed will be required to make use of this technique. We expect that offloading processor-intensive tasks onto FPGAs will provide the necessary computational improvement.

Acknowledgement

The work described in this paper was carried out by the Jet Propulsion Laboratory, California Institute of Technology, under a contract with the National Aeronautics and Space Administration. The authors thank Mr. Jan Tarsala for several useful discussions on PLL loop filter design and optimization.

References

[1] K. B. Cooper, R. J. Dengler, N. Llombart, T. Bryllert, G. Chattopadhyay, E. Schlecht, J. Gill, C. Lee, A. Skalare, I. Mehdi, P. H. Siegel, "Penetrating 3D Imaging at 4 and 25 Meter Range Using a Submillimeter-Wave Radar," *IEEE Trans. Microwave Theory and Tech.*, vol. 56, pp. 2771-2778, Dec. 2008.

[2] A. Maestrini, J. S. Ward, J. J. Gill, H. S. Javadi, E. Schlecht, C. Tripon-Canseliet, G. Chattopadhyay, I. Mehdi, "A 540-640-GHz High-Efficiency Four-Anode Frequency Tripler," *IEEE Trans. Microwave Theory and Tech.*, vol. 53, no. 9, pp. 2835-2843, Sep. 2005.

[3] L. Samoska, T. Gaier, A. Peralta, S. Weinreb, J. Bruston, I. Mehdi, Y. C. Chen, H. H. Liao, M. Nishimoto, R. Lai, H. Wang, Y. C. Leong, "MMIC Power Amplifiers as Local Oscillator Drivers for FIRST", *Proc. SPIE*, vol. 4013, pp. 275-284, 2000.

[4] H. Wang, L. Samoska, T. Gaier, A. Peralta, H.-H. Liao, Y. C. Leong, S. Weinreb, Y. C. Chen, M. Nishimoto, R. Lai, "Power-Amplifier Modules Covering 70-113 GHz Using MMICs," *IEEE Trans. Microwave Theory and Tech.*, vol. 49, pp. 9-16, 2001.

[5] Analog Devices, One Technology Way, Norwood MA 02062.

[6] Applied Radio Labs, P.O. Box 542, Beecroft NSW 2119, Australia